Large tunneling magnetoresistance in spin-filtering 1T-$MnSe_2$/h-BN van der Waals magnetic tunnel junction

Zhao Chen,[†] Xiaofeng Liu,[†] Xingxing Li,[‡] Pengfei Gao,[¶] ZhongJun Li,[†,§] Weiduo Zhu,[†] Haidi Wang,[*,†] and Xiangyang Li[*,‖,‡]

†*Department of Physics, Hefei University of Technology, Hefei, Anhui 230009, China*

‡*Department of Chemical Physics, Hefei National Laboratory for Physical Sciences at Microscale, University of Science and Technology of China, Hefei, Anhui 230026, China*

¶*Interdisciplinary Center for Fundamental and Frontier Sciences, Nanjing University of Science and Technology, Jiangyin, Jiangsu, 214443, China*

§*State Key Laboratory of Quantum Optics and Quantum Optics Devices, Shanxi University, Taiyuan 030006, China*

‖*School of Materials Science and Engineering, Anhui University, Hefei, Anhui 230601, China*

E-mail: haidi@hfut.edu.cn; xyangli@ustc.edu.cn

Supporting Information

Antiparallel magnetic configuration

In previous work,[1] it can be seen the conventional memory element design in magnetic tunnel junctions (MTJs). The bottom and top ferromagnetic layer are separated by inserting a thin tunnel layer. Then, switching between the parallel and antiparallel state of top ferromagnetic layer is achieved by using magnetic fields, when the bottom ferromagnetic layer is pinned by antiferromagnetic layer. Similarly, the multiple 1T-$MnSe_2$ ferromagnetic layers are divided into three magnetic regions by inserting h-BN layer as tunnel layers. As shown in Figure S1, the magnetic coupling between 1T-$MnSe_2$ layers is weakened by inserting h-BN. Furthermore, the magnetization of top and bottom 1T-$MnSe_2$ layers can be fixed to the antiparallel state by AFM layers. In general, although antiparallel order is not the magnetic ground state, it can be realized as initial antiparallel magnetic order in 1T-$MnSe_2$/h-BN/1T-$MnSe_2$/h-BN/1T-$MnSe_2$ junction. The AFM layers (pinning layers) may also have significant effects on transport properties. It is suggested that the pinned layers could grow outside of the transport region, and the pinning layers grow behind of the pinned layers in the non-transport region (Figure S2). In the non-transport region, the magnetic moment direction of the pinned layer is fixed by the pinning layer (AFM layer) through the exchange bias effect.[2] Meanwhile, the magnetic moment direction of the pinned layer in the transport region is fixed and parallel to that of the non-transport region for the intralayer ferromagnetic coupling of the pinned layer. Through the designed model, we can see that the pinning layers do not participate in the transport process, which is beneficial for ensuring the transport performance of MTJ.

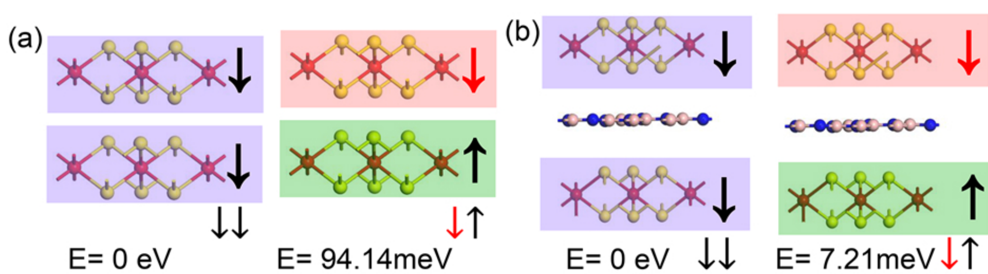

Fig. S 1: Magnetic configurations and energy of magnetic configurations for (a) bilayer 1T-$MnSe_2$ (b) 1T-$MnSe_2$/h-BN/1T-$MnSe_2$.

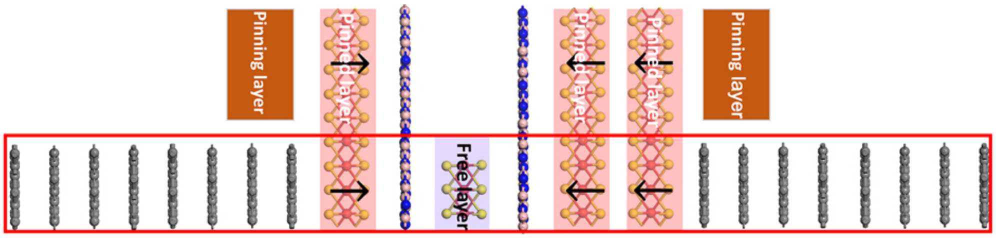

Fig. S 2: Schematic of the MTJ device model with the pinning layers. The red box is the transport region.

The spin-resolved conductance calculated with two basis sets

For testing error bar, the improvement of double-zeta double-polarized (DZDP) basis sets are adopted for junction to calculate conductance. As shown in Table S1, it can be seen that conductance involving DZDP basis sets is in the same order of magnitude as that using double-zeta polarized (DZP) basis sets. Thus, for graphene/1T-$MnSe_2$/h-BN/1T-$MnSe_2$/h-BN/1T-$MnSe_2$/graphene junction, the DZP basis sets are sufficient for accurate computations.

Table S 1: The spin-resolved conductance (10^{-10}e^2/h) of three magnetic configurations of device

	$G^{\uparrow}_{\mathrm{APC-DOWN}}$	$G^{\downarrow}_{\mathrm{APC-DOWN}}$	$G^{\uparrow}_{\mathrm{APC-UP}}$	$G^{\downarrow}_{\mathrm{APC-UP}}$	$G^{\uparrow}_{\mathrm{PC}}$	$G^{\downarrow}_{\mathrm{PC}}$
DZP	0.37	48.25	3.43	7.88	0.09	466.52
DZDP	0.16	60.35	1.26	4.37	0.09	448.39

The conductance calculated with lattice vibration

Phonons can cause atoms in the structure to deviate from the equilibrium position, resulting in changes in transport properties. To reduce the computation workload, we generated four structures with random displacements to describe lattice vibrations and directly study their multifold effects on spin-dependent transport. Firstly, the random displacement of atom positions is used to simulate lattice vibrations or phonons. In detail, the random displacement of atom positions for 1T-$MnSe_2$ and h-BN layers is 0.5 Å, while C atoms are fixed for high Young's modulus and strength of graphene.[3] We generated four structures of the junction with random displacements. Next, we use the ATK package, based on the non-equilibrium Green's function-density functional theory (NEGF-DFT) method,[4,5] to calculate the spin-dependent transport. The results show that the lattice vibration could cause a slight change in conductance (Figure S3) of the ↓↓↑↑, ↓↓↓↑ and ↓↓↓↓ states, but not an order of magnitude change.

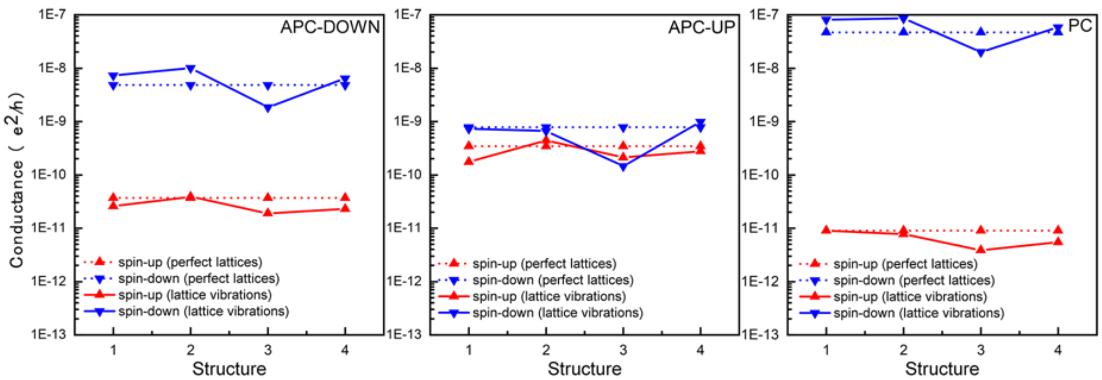

Fig. S 3: The spin-resolved conductance of three magnetic configurations with perfect lattices and lattice vibrations.

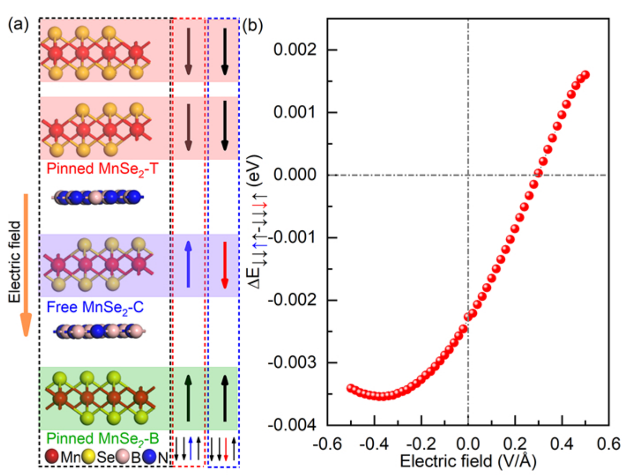

Fig. S 4: Side views of bilayer 1T-$MnSe_2$/h-BN/1T-$MnSe_2$/h-BN/1T-$MnSe_2$ junction, (b) energy differences between ↓↓↑↑ and ↓↓↓↑ states by the applied electric field.

The spin-resolved transport performances of graphene/ 1T-MnSe$_2$/h-BN/1T-MnSe$_2$/h-BN/1T-MnSe$_2$/graphene junction

In graphene/ 1T-MnSe$_2$/h-BN/1T-MnSe$_2$/h-BN/1T-MnSe$_2$/graphene junction (three-layer model), the transmission coefficient (conductance) of spin-down (spin-up) channel is much larger than those of spin-up (spin-down) channel in the $\downarrow\downarrow\uparrow$ ($\downarrow\uparrow\uparrow$) state, leading to a large spin polarized current (Figure S5). On the other hand, TMR is one of an important index to evaluate the performance of MTJs. The TMR$_e$ ratio of the three-layer model could be calculated as

$$\mathrm{TMR_e} = \frac{I/G_{\downarrow\downarrow\uparrow} - I/G_{\downarrow\uparrow\uparrow}}{I/G_{\downarrow\uparrow\uparrow}} \times 100\% \tag{1}$$

where $I/G_{\downarrow\downarrow\uparrow}$ and $I/G_{\downarrow\uparrow\uparrow}$ are the current /conductance of the $\downarrow\downarrow\uparrow$ and $\downarrow\uparrow\uparrow$ states, respectively. The density of states (DOS) in the spin-down and spin-up channels are reversed in the $\downarrow\downarrow\uparrow$ and $\downarrow\uparrow\uparrow$ states (Figure 1(c-d)), resulting in the transmission coefficient (conductance) of the spin-down and spin-up channels are reversed in the $\downarrow\downarrow\uparrow$ and $\downarrow\uparrow\uparrow$ states (Figure S5(d-e)). The total conductance of two spin channel in the $\downarrow\downarrow\uparrow$ state is the almost the same as that in the $\downarrow\uparrow\uparrow$ states. Thus, the TMR$_e$ ratio is approximately zero for this junction. Considering the manipulation of the magnetic states by the applied magnetic field, the magnetic moments of right 1T-MnSe$_2$ monolayer are fixed. The magnetic moments of the middle and left 1T-MnSe$_2$ layers are parallel with the external magnetic field. When the magnetic field direction is parallel to the magnetic moment direction of the pinned layer, it is labeled as $\uparrow\uparrow\uparrow$ state. When it is opposite, the magnetic state is labeled as $\downarrow\downarrow\uparrow$ state. The TMR$_m$ ratio of the junction could be calculated as

$$\mathrm{TMR_m} = \frac{I/G_{\uparrow\uparrow\uparrow} - I/G_{\downarrow\downarrow\uparrow}}{I/G_{\downarrow\downarrow\uparrow}} \times 100\% \tag{2}$$

where $I/G_{\uparrow\uparrow\uparrow}$ and $I/G_{\downarrow\downarrow\uparrow}$ are the current /conductance of the $\uparrow\uparrow\uparrow$ and $\downarrow\downarrow\uparrow$ states, respectively. The conductance of the device is summarized in Table S2. At the equilibrium

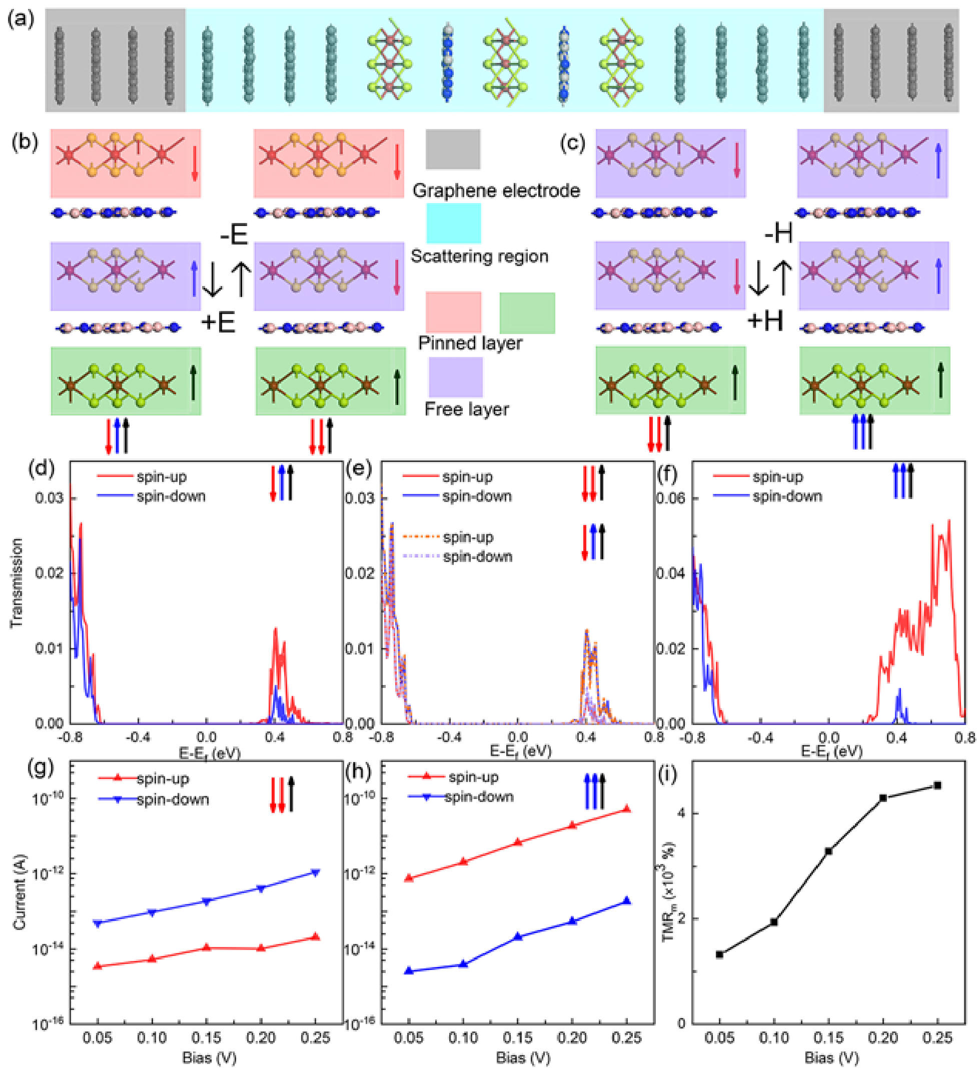

Fig. S 5: Magnetic configuration and structural model of three-layer model. Side view of 1T-$MnSe_2$/h-BN/1T-$MnSe_2$/h-BN/1T-$MnSe_2$ MTJ. By changing the direction of the applied electric field and magnetic field, the magnetic moments of center 1T-MnSe2 layer could be reversed between the ↓↑↑ and the ↓↓↑ state for (b), the ↓↓↑ state and the ↑↑↑ state for (c). Spin-resolved transmission spectra of the device in the ↓↑↑ (d), ↓↓↑ (e) and ↑↑↑ (f) states. The arrows denote the magnetic moments of the magnetic layer. The bias dependence of the spin-current in the ↓↓↑ state (g) and ↑↑↑ state (h), and (i) TMR_m for the three-layer model.

state, the spin-resolved transmissions spectra of the ↑↑↑ and ↓↓↑ states are shown in Figure S5(f,d). It is observed that the transmission coefficient of the spin-up channel in the ↑↑↑ state is several orders of magnitude larger than those of spin-down channel in the ↓↓↑ state, leading to a large TMR_m (2.75×10^2%). When the bias increases from 0.05 V to 0.25 V, the current of ↑↑↑ increases faster than that of ↓↓↑, leading to a large TMR_m ratio (4.53×10^3%).

Table S 2: The spin-resolved conductance (10^{-10}e^2/h) of thwo magnetic configurations of device

	↓↓↑	↑↑↑
$G^{\uparrow}$	24.15	1160.62
$G^{\downarrow}$	285.75	2.67

References

(1) Zhu, J.-G. J.; Park, C. Magnetic tunnel junctions. *Mater. Today* **2006**, *9*, 36–45.

(2) Ohldag, H.; Scholl, A.; Nolting, F.; Arenholz, E.; Maat, S.; Young, A.; Carey, M.; Stöhr, J. Correlation between exchange bias and pinned interfacial spins. *Phys. Rev. Lett.* **2003**, *91*, 017203.

(3) Lee, J.-U.; Yoon, D.; Cheong, H. Estimation of Young's modulus of graphene by Raman spectroscopy. *Nano Lett.* **2012**, *12*, 4444–4448.

(4) Brandbyge, M.; Mozos, J.-L.; Ordejón, P.; Taylor, J.; Stokbro, K. Density-functional method for nonequilibrium electron transport. *Phys. Rev. B* **2002**, *65*, 165401.

(5) Taylor, J.; Guo, H.; Wang, J. Ab initio modeling of quantum transport properties of molecular electronic devices. *Phys. Rev. B* **2001**, *63*, 245407.